11-1-2009

Investigation of the Physical and Electronic Properties of Indium Doped Zinc Oxide Nanofibers Synthesized by Electrospinning

A. F. Lotus

Y. C. Kang

R. D. Ramsier

George G. Chase
University of Akron Main Campus, gchase@uakron.edu

Investigation of the physical and electronic properties of indium doped zinc oxide nanofibers synthesized by electrospinning

A. F. Lotus
Department of Chemical and Biomolecular Engineering, The University of Akron, Akron, Ohio 44325-3906

Y. C. Kang
Department of Chemistry, Pukyong National University, Busan 608-737, Korea

R. D. Ramsier
Department of Physics, The University of Akron, Akron, Ohio 44325-4001 and Department of Chemistry, The University of Akron, Akron, Ohio 44325-360

G. G. Chase[a)]
Department of Chemical and Biomolecular Engineering, The University of Akron, Akron, Ohio 44325-3906

(Received 28 January 2009; accepted 14 September 2009; published 22 October 2009)

Nanostructured metal oxides and particularly nanofiber based materials can provide significant advances for the miniaturization of electronic, optoelectronic, photonic, sensor, and energy conversion devices with enhanced performance based on their unique material properties. In this study, indium doped zinc oxide (IZO) nanofibers were synthesized by electrospinning. These nanofibers have diameters in the range 50–100 nm. The effects of indium addition on the structural, optical, and electrical properties of the zinc oxide nanofiber matrices were investigated. The IZO nanofibers undergo significant changes in their optical and electrical properties compared to undoped zinc oxide nanofibers. © *2009 American Vacuum Society.* [DOI: 10.1116/1.3244588]

I. INTRODUCTION

Zinc oxide (ZnO) is a multifunctional material, which has been widely used for various applications such as, varistors,[1,2] transistors,[3] sensors,[4–6] piezoelectric devices,[7] solar cell windows,[8] UV and blue light emitting devices,[9] and surface acoustic wave devices.[10,11] ZnO films, in particular, are attracting more attention as transparent conductive films and gas sensors because of their wide availability, amenability to doping, low cost, nontoxicity and hence easy handling, and stability in hydrogen atmospheres.[12,13]

Different physical as well as chemical techniques have been employed to prepare undoped and doped ZnO films, e.g., vacuum evaporation,[14] spray pyrolysis,[15–17] rf magnetron sputtering,[18–21] sol-gel methods,[22,23] pulsed laser deposition,[24,25] metal-organic chemical vapor deposition,[26,27] and molecular beam epitaxy.[28] In this article, the preparation and characterization of indium doped ZnO by electrospinning are described. The electrospinning technique has the advantage of low cost, ease of use, safety, and has the potential to be implemented for large area deposition. The primary motivation for doping indium into ZnO is wavelength tunability for optoelectronic applications, although doping also results in marked changes in the electrical properties of ZnO as demonstrated in this work. Modifications of the crystal structure, optical absorption properties, electrical conductivity, and chemical makeup brought about by doping on the zinc oxide nanofibers are studied. These indium doped zinc oxide nanofibers have potential applications in catalytic, photocatalytic, photonic, electronic, sensor, and solar energy conversion devices.

II. EXPERIMENTAL DESCRIPTION

The IZO nanofibers were synthesized by adding sol-gel precursors to a polymer solution followed by electrospinning. The main features of the electrospinning system are fully described elsewhere.[29–31] For the preparation of zinc oxide precursor solutions, zinc acetate [$Zn(CH_3COO)_2$, Aldrich, 99.99% purity] was dissolved in de-ionized water at a mass ratio of 1:4. A polyvinylpyrrolidone (PVP, Aldrich)-ethanol (Pharmco) solution with a mass ratio of 1:6 (PVP: ethanol) was added to the aqueous zinc acetate solution at a mass ratio of 1.5:1 to provide adequate viscosity necessary for electrospinning. The indium precursor solution was prepared by dissolving indium chloride ($InCl_3$, Alfa-Aesar, 99.99% purity) in de-ionized water at a mass ratio of 1:4. All the solutions mentioned above were magnetically stirred for 24 h at room temperature.

The amount of aqueous indium chloride in the electrospinning solution was varied according to the desired level of doping. The In concentrations $(In/In+Zn)\times 100\%$ in the four different starting solutions were 0, 1.00, 1.75, and 6.50 at. %. Each solution was magnetically stirred for 1 h at room temperature before electrospinning to synthesize nanofibers.

The solutions were electrospun at a potential difference of 20 kV and a constant solution flow rate of 5 μl/min with a 20 cm distance from the needle tip to the fiber collector. The resultant fibers were heated to 873 K at a heating rate of

[a)]Author to whom correspondence should be addressed; electronic mail: gchase@uakron.edu

TABLE I. Physical characteristics of four different IZO nanofiber materials after calcining at 873 K for 5 h.

Sample	Atomic ratio in electrospinning solution, $\frac{In}{In+Zn}\times 100\%$	Grain size (nm)	Volume of the unit cell (Å^3)	Increased Volume by 1 at. % of In (Å^3)	Optical bandgap (eV)	Conductivity $\times 10^3$ (S/cm)
ZnO (Undoped)	0	40.78	47.58	0	3.37 ± 0.02	0.02 ± 0.002
IZO1	1.00	41.10	47.60	0.50	3.32 ± 0.02	3.27 ± 0.08
IZO2	1.75	41.85	47.69	0.54	3.20 ± 0.02	4.63 ± 0.35
IZO3	6.50	41.98	47.85	0.53	3.15 ± 0.03	6.74 ± 0.42

10 K/min and then kept at 873 K for 5 h to yield ceramic nanofibers. Compositions and characteristics of the four different IZO samples used in this investigation are summarized in Table I.

III. RESULTS AND DISCUSSION

A. Electron microscopy analysis

The average fiber diameters and microstructures of different IZO nanofibers were obtained from scanning electron microscopy (Hitachi S-2150) and high resolution transmission electron microscopy (Technai F30). Figure 1 shows a representative scanning electron microscopy (SEM) image of IZO nanofibers calcined at 873 K. The average diameter for these IZO nanofibers was determined to be approximately 80 nm. There was no significant change in the average diameters of zinc oxide nanofibers with varying indium additives in the nanofiber matrix. Figure 2 shows the representative high-resolution transmission electron microscopy (HRTEM) images of IZO nanofibers. HRTEM images reveal that the IZO nanofibers are highly crystalline and composed of single crystalline grains 20–30 nm in diameter.

B. X-ray diffraction analysis

Structural identification of the electrospun IZO nanofibers calcined at 873 K was carried out using x-ray powder diffraction patterns obtained with a Philips diffractometer employing Cu Kα radiation, with 2θ in the range 10°–60°. The diffraction patterns of different IZO nanofiber samples are presented in Fig. 3. The x-ray diffraction (XRD) patterns indicate that all of the nanofiber structures are well crystallized after calcination at 873 K for 5 h. The diffraction peaks for the zinc-based nanofiber materials in Fig. 3 are consistent with the hexagonal zinc oxide crystal structure reported in literature.[32] The grain size D was calculated from the (101) peak width using Scherrer's formula

$$D = \frac{K\lambda}{B\cos\theta},$$

where D, λ, θ, and B are the mean crystallite size, the x-ray wavelength, the Bragg diffraction angle, and the full width half maximum (FWHM) of the (101) diffraction peak, respectively. No diffraction peaks of any other structure such as In_2O_3 or $In(OH)_3$ were found in the zinc oxide nanofiber matrix. The microstructural parameters of the four different nanofiber samples based on the XRD patterns are given in Table I. The size distribution calculated from the XRD data is slightly larger than the results obtained from HRTEM micrographs. This difference in size distribution arises due to the fact that TEM measured area weighted grain size distribution, while XRD measured volume averaged size distribution. The grain size was found to increase monotonically with the increase in indium concentrations. The result could indicate the substitution of Zn atom (ionic radius, r_{Zn} is

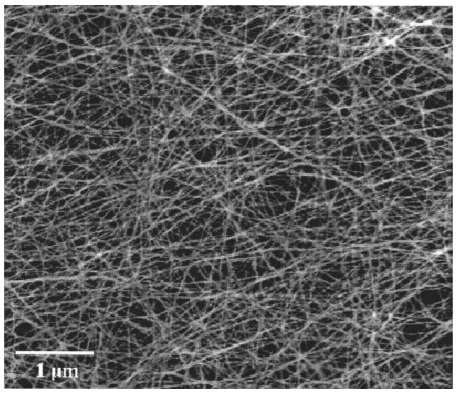

FIG. 1. Representative SEM image of indium doped zinc oxide nanofibers (IZO2 material) exhibiting an average fiber diameter of approximately 80 nm after being calcined at 873 K for 5 h.

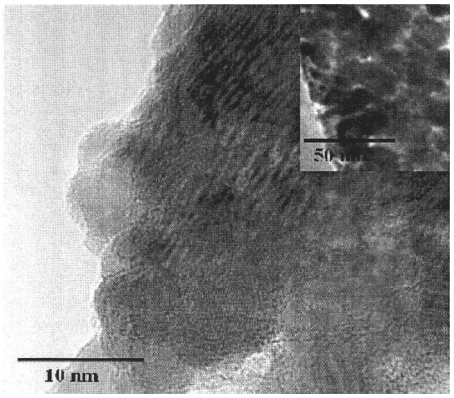

FIG. 2. HRTEM images of indium doped zinc oxide nanofibers (IZO2 material) after being calcined at 873 K for 5 h.

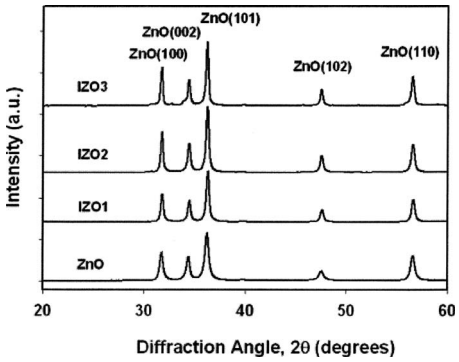

FIG. 3. XRD patterns of undoped and indium doped zinc oxide nanofibers calcined at 873 K for 5 h.

0.74 Å) by larger In atom (r_{In} is 0.80 Å) into the ZnO lattice at low indium concentrations, followed by possible segregation of In additives at the grain boundaries at the highest concentration. The lattice parameters are listed in Table I. The increase in the unit cell dimensions for the doped samples (relative to the starting material) is consistent with the notion of induced strain by the dopant and the maximum microstrain was measured in the order of 0.002.

C. Ultraviolet-visible spectroscopy

A Cary 300 spectrophotometer was used to obtain ultraviolet-visible (UV-Vis) diffuse reflectance spectra of the IZO nanofibers. Samples were ground to a fine powder and packed into a shallow stainless steel sample plaque. The optical diffuse reflectances of the samples were measured in the wavelength range 200–800 nm. Figure 4 shows representative spectra for different IZO nanofiber samples. Based on these reflectance spectra, the absorption edge for each material was determined by the first derivative method. Using the calculated absorption edge values, the band gap energies were calculated as 3.37 eV for undoped ZnO nanofibers and 3.32, 3.20, and 3.15 eV for the three doped samples (IZO1, IZO2, and IZO3), respectively, using the relationship of photon energy and frequency $E=h\nu$, where h is Planck's constant (6.626×10^{-34} J s) and $\nu=c/\lambda$, where c is the speed of light (2.998×10^{8} m/s) and λ is the wavelength of light. The variation in the optical bandgap energy can be attributed to perturbation of the carrier concentration in the conduction band arising from In doping on ZnO as observed in some previous studies.[33,34] The optical bandgap of the four different samples calculated from the absorption edges are given in Table I.

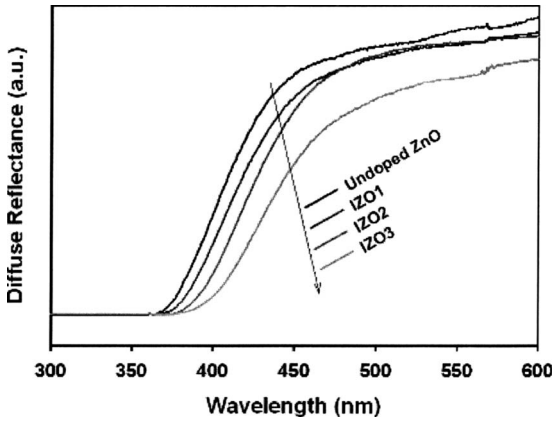

FIG. 4. UV-Vis spectra of undoped and indium doped zinc oxide nanofibers calcined at 873 K for 5 h.

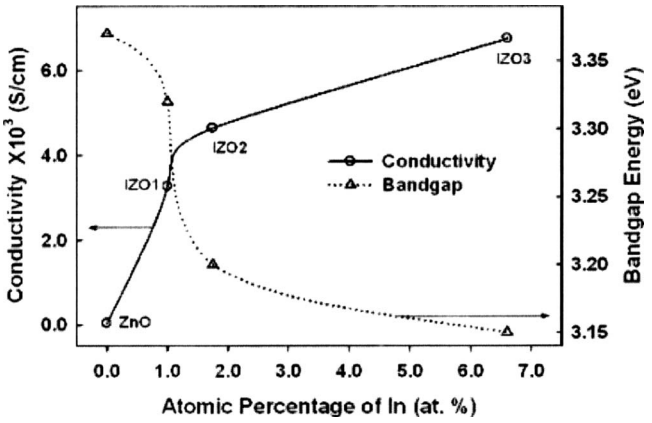

FIG. 5. Electrical conductivities and optical bandgap energies of undoped and indium doped zinc oxide nanofibers calcined at 873 K for 5 h.

D. Current-voltage (*I-V*) and conductivity measurements

The electrical properties of the IZO nanofibers were investigated using a Keithley 2410 sourcemeter. IZO nanofibers were ground and formed into pellets (6 mm diameter and 0.75 mm thickness) at a hydrostatic pressure of 45 MPa to measure the electrical conductivity. A thin layer of nickel metal with a thickness of 100 nm was deposited on the flat surfaces of the pellet using plasma enhanced physical vapor deposition (PEPVD) to minimize contact resistance. The nickel coated IZO pellets were placed on an insulating glass slide and electrical contacts were made with silver paste at the two flat surfaces using Ag wires.

The conductivities (σ, S/cm) of the IZO materials were calculated using the resistance R obtained from the I-V measurement, length L, and cross sectional area A of the pellets as $\sigma=L/RA$. Figure 5 shows the conductivity and optical bandgap energies of different IZO nanofibers at room temperature. Compared to the undoped zinc oxide nanofibers, the IZO materials exhibit enhanced electrical conductivity. This tendency could be explained based on the incorporation of In atoms into the ZnO lattice, during the crystal growth process in the following manner. As the In concentration in the solution increases, more and more In atoms occupy Zn sites, and an electron is donated to every In atom, increasing the carrier concentration. Since the solid solubility limit of the indium content in ZnO is about 2 at. %, it is probable that segregation of indium is occurring at least in the IZO3 materials, perhaps as indium oxide in the grain boundaries.

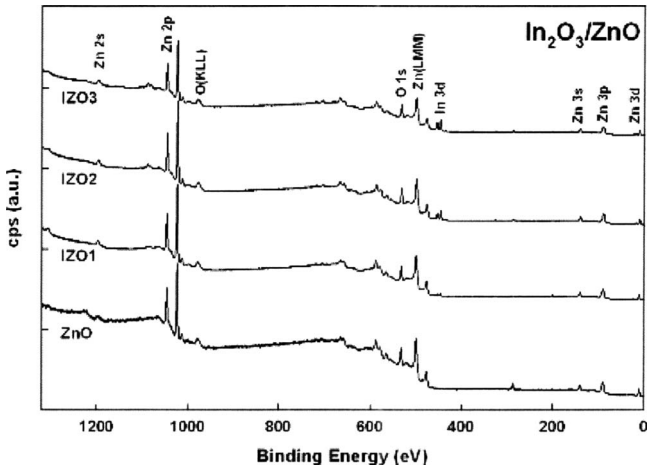

FIG. 6. Survey XP spectra of undoped (ZnO) and IZO nabofibers.

E. X-ray photoelectron spectroscopy

X-ray photoelectron spectroscopy (XPS) (VG ESCALAB MK II, West Sussex, UK) was used to study of the chemical nature of the IZO nanofibers. The base pressure in the analysis chamber was kept less than 1×10^{-9} mbar. A twin anode x-ray source Mg $K\alpha$ (1253.6 eV) and Al $K\alpha$ (1486.6 eV), and a concentric hemispherical analyzer are housed in the XPS system. During all experiments discussed here, XP spectra were obtained using the Al $K\alpha$ x-ray source. The parameters used for XPS experiments were an anode voltage of 9 kV, an electron multiplier voltage of 2850 eV, anode current of 20 mA, filament current of 4.2 A, pass energy of 50 eV, dwell time of 100 ms, and energy step size of 0.5 eV in constant analyzer energy mode for survey scans. High resolution scans were performed at an energy step size of 0.02 eV and a pass energy of 20 eV with all other parameters the same as used in survey scans.

The survey XP spectra of undoped zinc oxide and IZO nanofibers are shown in Fig. 6. As the content of indium increased, the indium 3*d* doublet XP feature (445–455 eV) grows in intensity as expected.[35,36] In addition to the Zn 2*p* doublet peaks between 1020 and 1050 eV and O 1*s* singlet feature near 530 eV that were observed, the adventitious C 1*s* peak near 285 eV was also detected.

For detailed study of the IZO nanofibers, high resolution XP scans were performed in the binding energy ranges of indium 3*d*, oxygen 1*s*, and zinc 2*p* states. Figures 7(a)–7(c) show the high resolution XP spectra of In 3*d*, O 1*s*, and Zn 2*p* regions of IZO nanofibers, respectively. Charging effects were corrected using the C 1*s* peak of drift carbon at 284.6 eV as a reference.[37] As the atomic percentage of indium in the starting solution increased from 1.0% to 6.5%, the In 3*d* doublet XP feature [in Fig. 7(a)] grew in intensity. The peak intensities of the O 1*s* and Zn 2*p* features shown in Figs. 7(b) and 7(c), respectively, did not change significantly, but the peak shapes and peak positions changed.

The peaks were not symmetric in the high resolution XP spectra for indium and zinc in our electrospun nanofibers. The phenomena implied that multiple oxidation states of indium and zinc exist in the samples. To understand the oxidation states, peak deconvolution was performed for In $3d_{5/2}$, O 1*s*, and Zn $2p_{3/2}$ and the results are shown in Figs. 8(a)–8(c), respectively. In the peak deconvolution process, only In $3d_{5/2}$ and Zn $2p_{3/2}$ were analyzed instead of the full doublet peaks because large spin-orbit splitting constants are large (7.54 and 23 eV, respectively).[38] The FWHMs used for peak deconvolution are 2.1 ± 0.1, 2.0 ± 0.1, and 2.1 ± 0.1 eV for In $3d_{5/2}$, O 1*s*, and Zn $2p_{3/2}$, respectively, using XPSPEAK program (ver. 4.1). After the deconvolution process, two oxidation states were assigned for indium species: one for metallic indium at a binding energy of 444.5 ± 0.2 eV and one for indium oxide at around 445.1 ± 0.1 eV. These assigned val-

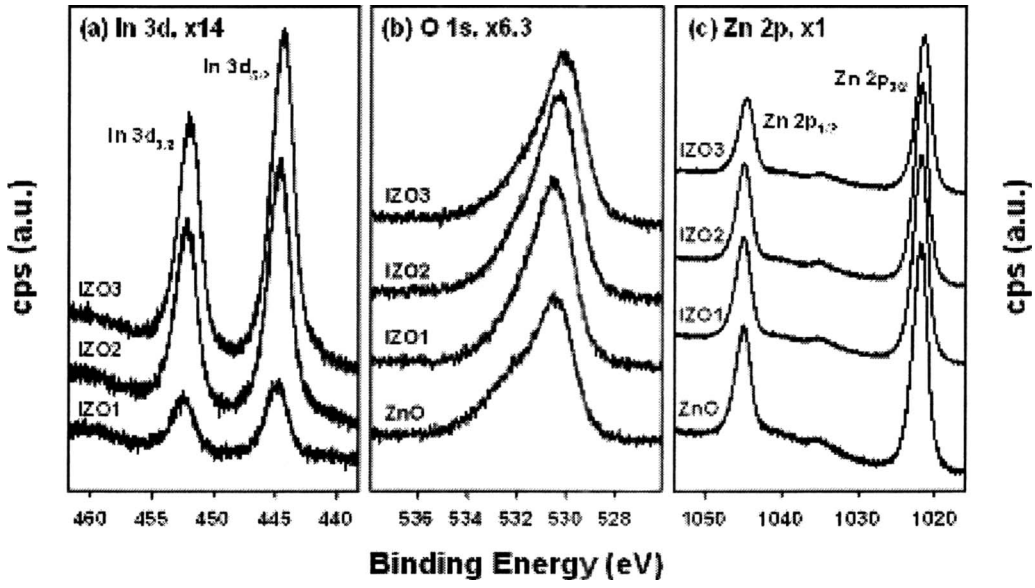

FIG. 7. High resolution XP spectra of undoped and indium doped zinc oxide nanofibers of the In 3*d* region (a), O 1*s* region (b), and Zn 2*p* region (c). The relative scales of the spectra are shown after the title of the figures.

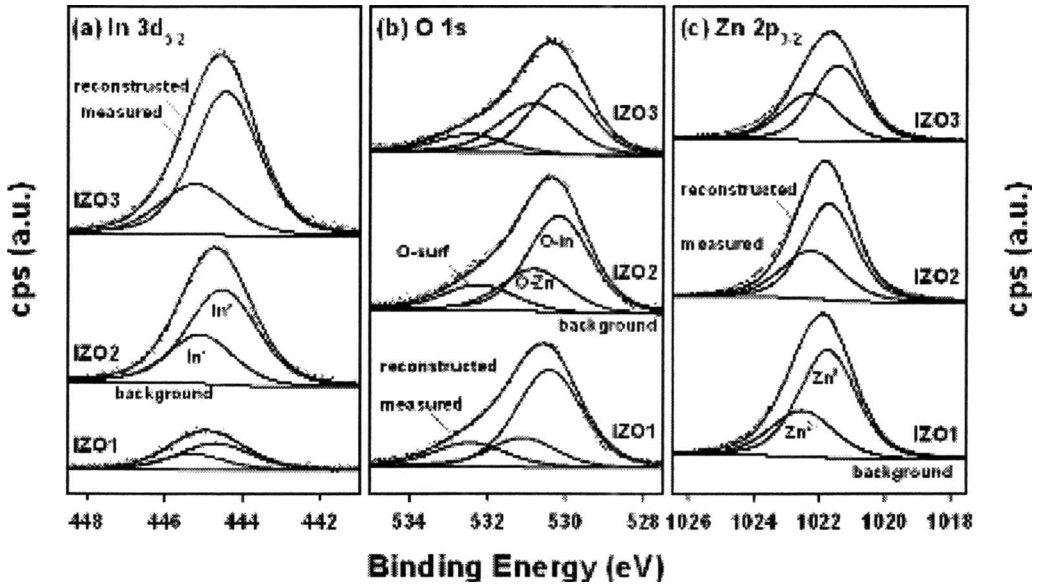

FIG. 8. Deconvoluted high resolution XP spectra of indium doped zinc oxide nanofibers of the In $3d_{5/2}$ region (a), O 1*s* region (b), and Zn $2p_{3/2}$ region (c). The Shirley backgrounds were applied to all spectra for peak deconvolution. In (a), metallic indium at a binding energy of 444.5 eV and In^{3+} at around 445.1 are assigned. In (b), the assigned binding energies for oxygen are 530.2 eV for O–In, 530.9 eV for O–Zn, and 532.3 eV for surface hydroxide. In (c), the assigned binding energies are Zn^0 at 1021.6 eV and ZnO at 1022.3 eV.

ues are in good agreement with the reported binding energy.[35]

Two oxidation states were assigned for zinc species: one for Zn^0 at a binding energy of 1021.6 ± 0.1 eV and the other for Zn^{2+} at around 1022.3 ± 0.2 eV.[39] Three oxidation states were assigned for oxygen species: one for O–In at a binding energy of 530.2 ± 0.2 eV,[35] for O–Zn at around 530.9 ± 0.2 eV,[40] and for surface oxygen at around 532.3 ± 0.1 eV.[41,42] As the indium content increased from 1.0% to 6.5%, the ratio of In^0 to In^{3+} increased from 1.86 to 2.58 but the ratio of Zn^0 to Zn^{2+} decreased from 2.10 to 1.44, as shown in Figs. 8(a) and 8(c). This phenomenon could be explained by zinc acting as a reducing agent with a lower reduction potential (−0.764 V) compare to that of indium (−0.338 V).[43] It is reasonable to conclude that zinc was oxidized while indium was reduced spontaneously as the indium content increased. This is supported by the ratio of oxygen species shown in Fig. 8(b). The percentage of O–Zn increased from 19.3% to 38.8% and that of O–In decreased from 63.3% to 55.0% as the indium content of the IZO materials was raised.

Figure 9 shows the valence band region of XP spectra of our electrospun nanofibers. The indium 4*d* feature (~17 eV) clearly grows as the indium content in IZO nanofibers increases as seen in Fig. 9(a). The peak center of the density of states near 0 eV [Fig. 9(b)] shifts to a lower binding energy with an increase in the indium content that is consistent with the increased conductivity data shown in Fig. 5.

IV. CONCLUSIONS

IZO nanofiber mats have been successfully prepared by electrospinning polymer solutions containing the sol-gel precursors followed by heating the fiber mats. XRD analysis shows typical patterns of the hexagonal ZnO structure for both doped and undoped ZnO nanofibers. The incorporation of In into the ZnO nanofiber matrix was verified by the XPS measurements. The optical bandgap energies of the different doped ZnO nanofibers varied from 3.15 to 3.37 eV, decreasing with the increased In concentration in the solution. Conductivity measurements show that incorporation of dopant-indium increased the conductivity of zinc oxide nanofibers two orders of magnitude consistent with changes in the electric structure and oxidation state of the materials. Electrospinning is found to be a simple, low cost method for dopant incorporation in the nanofiber matrix. It is therefore possible to bring about desirable changes in the structural, electrical, and optical properties of metal oxide nanofibers which can widen their applicability.

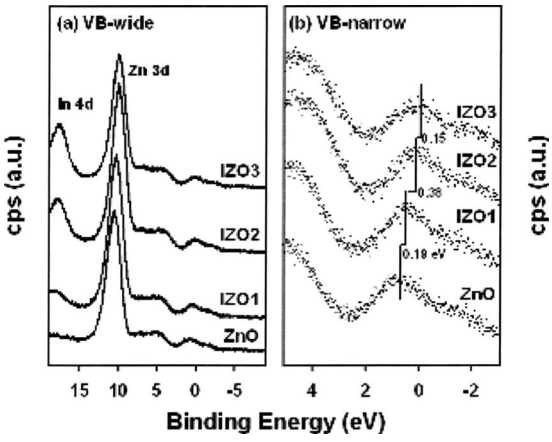

FIG. 9. High resolution XP spectra of the valence band region of undoped and indium doped zinc oxide nanofibers.

ACKNOWLEDGMENTS

This work was supported by the Coalescence Filtration Nanomaterials Consortium: Ahlstrom Paper Group, Donaldson Company, Cummins Filtration, Parker Hannifin, and MemPro Cermics Co. This work is also supported by the National Science Foundation under Grant No. DMI-0403835. We acknowledge Dr. Edward Evans for use of PEPVD equipment, Dr. Sasa Dordevic for his UV-Vis spectrophotometer, and Ms. Juyun Park for x-ray photoelectron spectroscopy assistance.

[1]K. Mukae, K. Tsuda, and I. Nagasawa, Jpn. J. Appl. Phys., Part 1 **16**, 1361 (1977).
[2]D. Fernandez-Hevia, J. de Frutos, A. C. Caballero, and J. F. Fernandez, Appl. Phys. Lett. **82**, 212 (2003).
[3]R. L. Hoffman, B. J. Norris, and J. F. Wager, Appl. Phys. Lett. **82**, 733 (2003).
[4]C. H. Kwon, H.-K. Hong, D. H. Yun, K. Lee, S.-T. Kim, Y.-H. Roh, and B.-H. Lee, Sens. Actuators B **25**, 610 (1995).
[5]H. Nanto, H. Sokooshi, and T. Kawai, Sens. Actuators B **14**, 715 (1993).
[6]S. Pizzini, N. Butta, D. Narducci, and M. Palladino, J. Electrochem. Soc. **136**, 1945 (1989).
[7]J. G. E. Gardeniers, Z. M. Rittersma, and G. J. Burger, J. Appl. Phys. **83**, 7844 (1998).
[8]S. Major and K. L. Chopra, Sol. Energy Mater. **17**, 319 (1988).
[9]D. M. Bagnall, Y. F. Chen, Z. Zhu, T. Yau, S. Koyama, M. Y. Shen, and T. Goto, Appl. Phys. Lett. **70**, 2230 (1997).
[10]G. S. Kino and R. S. Wagers, J. Appl. Phys. **44**, 1480 (1973).
[11]S. J. Chang, Y. K. Su, and Y. P. Shei, J. Vac. Sci. Technol. A **13**, 385 (1995).
[12]S. Major, S. Kumar, M. Bhatnagar, and K. L. Chopra, Appl. Phys. Lett. **49**, 394 (1986).
[13]J. Song, G.-H. Kang, K.-H. Yoon, W. Cho, and K.-S. Lim, Ungyong Mulli **7**, 387 (1994).
[14]A. Kuroyanagi, Jpn. J. Appl. Phys., Part 1 **28**, 219 (1989).
[15]A. Sanchez-Juarez, A. Tiburcio-Silver, A. Ortiz, E. P. Zironi, and J. Richards, Thin Solid Films **333**, 196 (1998).
[16]D. Goyal, P. Solanki, B. Marathe, M. Takwale, and V. Bhide, Jpn. J. Appl. Phys., Part 1 **31**, 361 (1992).
[17]K. T. Ramakrishna Reddy and R. W. Miles, J. Mater. Sci. Lett. **17**, 279 (1998).
[18]S. Takada, J. Appl. Phys. **73**, 4739 (1993).
[19]H. Nanto, H. Sokooshi, and T. Usuda, Sens. Actuators B **10**, 79 (1993).
[20]T. Minami, H. Nanto, and S. Takada, Jpn. J. Appl. Phys., Part 2 **24**, L605 (1985).
[21]K. Tominaga, H. Manabe, N. Umezu, I. Mori, T. Ushiro, and I. Nakabayashi, J. Vac. Sci. Technol. A **15**, 1074 (1997).
[22]M. Ohyama, H. Kozuka, and T. Yoko, Thin Solid Films **306**, 78 (1997).
[23]T. Tsuchiya, T. Emoto, and T. Sei, J. Non-Cryst. Solids **178**, 327 (1994).
[24]V. Craciun, J. Elders, J. G. E. Gardeniers, and I. W. Boyd, Appl. Phys. Lett. **65**, 2963 (1994).
[25]S. V. Prasad, J. J. Nainaparampil, and J. S. Zabinski, J. Vac. Sci. Technol. A **20**, 1738 (2002).
[26]N. D. Kumar, M. N. Kamala Sanan, and S. Chandra, Appl. Phys. Lett. **65**, 1373 (1994).
[27]A. C. Jones, S. A. Rushworth, and J. Auld, J. Cryst. Growth **146**, 503 (1995).
[28]H. J. Ko, T. Yao, Y. Chen, and S. K. Hong, J. Appl. Phys. **92**, 4354 (2002).
[29]J. Doshi and D. H. Reneker, J. Electrost. **35**, 151 (1995).
[30]D. H. Reneker, A. L. Yarin, H. Fong, and S. Koombhongse, J. Appl. Phys. **87**, 4531 (2000).
[31]A. Theron, E. Zussman, and A. L. Yarin, Nanotechnology **12**, 384 (2001).
[32]JCPDS Card No. 36-1451.
[33]K. J. Kim and Y. R. Park, Appl. Phys. Lett. **78**, 475 (2001).
[34]G. Yogeeswaran, C. R. Chenthamarakshan, N. R. de Tacconi, and K. Rajeshwar, J. Mater. Res. **21**, 3234 (2006).
[35]T. P. Nguyen, P. Le Rendu, and S. A. de Vos, Synth. Met. **138**, 113 (2003).
[36]P. Nguyen, S. Vaddiraju, and M. Meyyappan, J. Electron. Mater. **35**, 200 (2006).
[37]H. J. Borg, C. C. A. van den Oetelaar, L. J. van Ijzendoorn, and J. W. Niemantsverdriet, J. Vac. Sci. Technol. A **10**, 2737 (1992).
[38]*Handbook of X-ray Photoelectron Spectroscopy*, edited by J. Chastain, J. F. Moulder, W. F. Stickle, P. E. Sobel, and K. D. Bomben (Perkin-Elmer Corporation, Physical Electronics Division, Eden Prairie, MN , 1995).
[39]M. H. Shin, M. S. Park, S. H. Jung, J. H. Boo, and N.-E. Lee, Thin Solid Films **515**, 4950 (2007).
[40]N. Boulares, K. Guergouri, R. Zouaghi, N. Tabet, A. Lusson, F. Sibieude, and C. Monty, Phys. Status Solidi A **201**, 2319 (2004).
[41]G. L. Mar, P. Y. Timbrell, and R. N. Lamb, Chem. Mater. **7**, 1890 (1995).
[42]L.-J. Meng, C. P. Moreira de Sá, and M. P. dos Snatos, Appl. Surf. Sci. **78**, 57 (1994).
[43]D. C. Harris, *Quantitative Chemical Analysis*, 5th ed. (W. H. Freeman and Company, New York, 1999).